# Superconductivity mediated by quantum critical antiferromagnetic fluctuations: The rise and fall of hot spots

Xiaoyu Wang,[1] Yoni Schattner,[2] Erez Berg,[2] and Rafael M. Fernandes[1]
[1]*School of Physics and Astronomy, University of Minnesota, Minneapolis, Minnesota 55455, USA*
[2]*Department of Condensed Matter Physics, Weizmann Institute of Science, Rehovot 7610001, Israel*
(Received 13 December 2016; revised manuscript received 1 May 2017; published 25 May 2017)

In several unconventional superconductors, the highest superconducting transition temperature $T_c$ is found in a region of the phase diagram where the antiferromagnetic transition temperature extrapolates to zero, signaling a putative quantum critical point. The elucidation of the interplay between these two phenomena—high-$T_c$ superconductivity and magnetic quantum criticality—remains an important piece of the complex puzzle of unconventional superconductivity. In this paper, we combine sign-problem-free quantum Monte Carlo simulations and field-theoretical analytical calculations to unveil the microscopic mechanism responsible for the superconducting instability of a general low-energy model, called the spin-fermion model. In this approach, low-energy electronic states interact with each other via the exchange of quantum critical magnetic fluctuations. We find that even in the regime of moderately strong interactions, both the superconducting transition temperature and the pairing susceptibility are governed not by the properties of the entire Fermi surface, but instead by the properties of small portions of the Fermi surface called hot spots. Moreover, $T_c$ increases with increasing interaction strength, until it starts to saturate at the crossover from hot-spots-dominated to Fermi-surface-dominated pairing. Our work provides not only invaluable insights into the system parameters that most strongly affect $T_c$, but also important benchmarks to assess the origin of superconductivity in both microscopic models and actual materials.

DOI: 10.1103/PhysRevB.95.174520

## I. INTRODUCTION

In the two known families of high-temperature superconductors—the copper-based and the iron-based materials—the superconducting (SC) state is observed in close proximity to an antiferromagnetic (AFM) state [1–4]. In the particular cases of iron pnictides and electron-doped cuprates, the highest SC transition temperature $T_c$ takes place in the vicinity of a putative antiferromagnetic quantum critical point (QCP) [5–7], i.e., a continuous AFM phase transition that occurs at zero temperature (see Fig. 1). Although direct detection of such a QCP is difficult, some of its manifestations at nonzero temperatures, such as a nearly diverging magnetic correlation length, are experimentally observed [8,9]. These observations led to the proposal that quantum critical AFM fluctuations may provide the glue binding the Cooper pairs in an unconventional SC state [10–15], be it a nodal $d$-wave state, as in the case of the cuprates, or a nodeless $s^{+-}$-wave state, as in the case of the iron pnictides.

The reasoning behind this theoretical proposal can be understood from a straightforward extension of the conventional weak-coupling BCS theory for phonon-mediated $s$-wave superconductors. In contrast to the electron-phonon coupling, which causes an attractive pairing interaction that does not depend on momentum, AFM fluctuations generate a repulsive pairing interaction strongly peaked at the momentum corresponding to the AFM wave vector $\mathbf{Q}$ [1–4]. In this case, the BCS gap equations only admit a solution if the gap function $\Delta(\mathbf{k})$ changes its sign when the momentum is translated by $\mathbf{Q}$, i.e., $\Delta(\mathbf{k}+\mathbf{Q}) \propto -\Delta(\mathbf{k})$. As a result, depending on the Fermi surface geometry and on the wave vector $\mathbf{Q}$, different types of SC states are favored. While a $d$-wave state is obtained for a large Fermi surface and $\mathbf{Q} = (\pi,\pi)$, an $s^{+-}$-wave state arises for small Fermi pockets separated by $\mathbf{Q} = (\pi,0)/(0,\pi)$. Despite its appeal, such a weak-coupling BCS-like approach is not appropriate to describe these systems, since the proximity to a QCP renders the interactions strong and, on top of that, clouds the very concept of quasiparticles, which is a key property of a Fermi liquid [16].

Thus, while there is little question that AFM fluctuations can promote an unconventional SC state, the elucidation of the microscopic mechanisms involved remain a major challenge. Addressing this issue is important not only to assess the relevance of quantum critical pairing to high-$T_c$ materials, but also to establish which of the many system parameters should be ideally optimized to enhance $T_c$. To answer these important questions, microscopic models that are expected to display AFM and SC ground states have been widely studied, most notably the Hubbard model [17–20]. Alternatively, in the hope of elucidating universal features of quantum critical pairing, many works have focused on a general low-energy model in which the fermions associated with the low-energy electronic states interact with each other by exchanging magnetic fluctuations, which in turn arise from high-energy states; this is the so-called spin-fermion model [10,12]. Because these fluctuations are peaked at the AFM ordering vector $\mathbf{Q}$, not all low-energy states are equally affected by this interaction. More specifically, only states near the hot spots—special points on the Fermi surface that are displaced from each other by the AFM ordering vector $\mathbf{Q}$—can exchange AFM fluctuations while remaining near the Fermi level. This property lends support to the idea that the hot spots may play a primary role in driving the superconducting transition.

However, despite intense research activity in this front, the extent to which hot-spots properties govern the SC instability remains a hotly debated issue. One of the reasons is the difficulty in developing a controlled strong-coupling theory for the

 

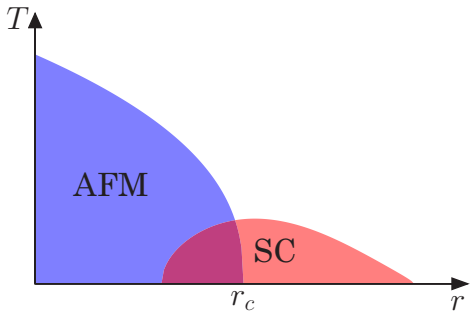


FIG. 1. Schematic phase diagram of the spin-fermion model. The antiferromagnetic (AFM) transition temperature is suppressed to zero at $r = r_c$, giving rise to a quantum critical point. According to the results of Ref. [25] for the spin-fermion model, a superconducting (SC) dome then appears, hiding the antiferromagnetic quantum critical point. The maximum $T_c$ is found very close to $r = r_c$.

spin-fermion model, which is ultimately related to the absence of a natural small parameter in the problem [12,21–23]. This situation is to be contrasted with the phonon-mediated pairing problem, where the clear separation between electronic and lattice energy scales ensures the existence of a controlled diagrammatic expansion—the celebrated Eliashberg theory.

In this paper, we combine extensive quantum Monte Carlo (QMC) simulations and analytical calculations to shed light on this problem. Our starting point is the two-band version of the two-dimensional spin-fermion model, in which the AFM fluctuations mediate interactions between electrons from two different bands. The choice of a two-band model is essential, because it does not suffer from the infamous sign problem generally present in QMC simulations [24]. While a recent study has established the existence of a SC dome peaked at the AFM quantum critical point of this model [25], similarly to Fig. 1, in this paper our goal is to elucidate the microscopic mechanism responsible for this SC state. Unveiling the pairing mechanism encoded in the spin-fermion model is fundamental to advance our understanding of the general problem of superconductivity in quantum critical systems for several reasons. First, the sign-problem-free QMC algorithm only works for the rather artificial two-band model. Establishing the solution of this two-band spin-fermion model, where the unbiased sign-problem-free QMC approach offers a unique benchmark for analytical approximations, is the most promising way to generalize the results to other types of band structures. Second, being a low-energy model, the main relevance of the spin-fermion model to the ongoing effort to search for higher $T_c$ materials is to provide robust trends for how changes in the various system parameters affect $T_c$; e.g., is the density of states at the Fermi level more important than the properties of the hot spots? Third, the spin-fermion model is one among several models that have been proposed to understand high-$T_c$ systems. Without knowing the precise predictions of this model, it is very hard to rule out or confirm that the physics encoded in the spin-fermion model is relevant to the real systems.

In this paper, our general goal is to establish the general solution of the spin-fermion model by a detailed comparison between numerics and analytics. To achieve this goal, we study a family of band dispersions that interpolate between closed nearly nested Fermi pockets to open Fermi surfaces, passing through a Van Hove singularity, where the density of states is strongly peaked. This nontrivial dependence of the density of states on the band dispersion allows us to separate phenomena associated with the Fermi surface as a whole and with the hot spots only. Tuning the system to its AFM quantum critical point, we extract from our QMC results both the superconducting transition temperature $T_c$, which in our two-dimensional system is a Berezinskii-Kosterlitz-Thouless transition, and the temperature dependence of the pairing susceptibility, $\chi_{\text{pair}}$. Similarly to previous works [24–26], we find that the favored SC state is the one in which the gap function changes sign from one band to the other, in qualitative agreement with the weak-coupling arguments given above. Our main results, however, are on the dependence of $T_c$ and $\chi_{\text{pair}}$ on the band dispersion parameters. Surprisingly, we find that $T_c$ is not sensitive to the density of states $N_f$, which displays a sharp enhancement near the Van Hove singularity. Instead, even when the interaction strength is comparable to the bandwidth, $T_c$ is found to depend only on the angle between the Fermi velocities of a pair of hot spots, $\sin\theta_{\text{hs}}$, via

$$T_c = A_c \lambda^2 \sin\theta_{\text{hs}}, \tag{1}$$

where $\lambda$ is the interaction parameter that couples magnetic and electronic degrees of freedom, and $A_c$ is a universal constant independent of the band dispersion. As for the pairing susceptibility, we show that the QMC data for all band dispersions collapse onto a single curve given by

$$\chi_{\text{pair}}(T) = A_{\text{pair}} f_{\text{pair}}\left(\frac{T}{T_c}\right), \tag{2}$$

where $f_{\text{pair}}(\frac{T}{T_c})$ is a universal function that does not depend on the band dispersion, whereas $A_{\text{pair}}$ is a constant that depends weakly on the band dispersion. Equations (1) and (2) are the main results of our paper, establishing that the hot-spots properties govern not only the SC transition temperature but also the temperature dependence of the SC fluctuations. To understand these results, we analytically study the spin-fermion model via a hot-spots Eliashberg approximation introduced in previous works for the one-band model [10,14]. Basically, this approximation consists of assuming that the magnetic degrees of freedom are much slower than the electronic ones, and that the hot spots govern the critical properties of the system. Despite being formally uncontrolled, this approximation not only gives the same functional dependence of the SC transition temperature on the spin-fermion parameters of Eq. (1), but it also captures very well the universal function $f_{\text{pair}}(x)$ obtained from the QMC results.

An immediate consequence of Eq. (1) is that $T_c$ would not have an upper limit upon increasing the interaction $\lambda$. We find, however, that when $\lambda^2$ becomes larger than the electronic bandwidth, $T_c$ stops increasing and nearly saturates to a value of the order of a few percent of the electronic bandwidth. Combined with our analytical investigation of the spin-fermion model, we attribute this behavior to the whole Fermi surface behaving as a "large hot spot," and to the failure of the hot-spots-only approximation [27]. Therefore, our results indicate that, within the spin-fermion model, the largest possible value

of $T_c$ does not depend on the interaction strength, and is first achieved at the crossover between hot-spots-dominated and Fermi-surface-dominated pairing.

## II. THE SPIN-FERMION MODEL

The spin-fermion model is a low-energy model widely employed to study universal properties of pairing mediated by AFM fluctuations [10,12,24]. It describes low-energy electronic degrees of freedom interacting with magnetic fluctuations that arise from high-energy degrees of freedom. In this work, we consider a two-dimensional model with two independent bands, yielding the following noninteracting Hamiltonian:

$$\mathcal{H}_0 = \sum_{\mathbf{k}\alpha} \varepsilon_{c,\mathbf{k}} c^\dagger_{\mathbf{k}\alpha} c_{\mathbf{k}\alpha} + \sum_{\mathbf{k},\alpha} \varepsilon_{d,\mathbf{k}} d^\dagger_{\mathbf{k}\alpha} d_{\mathbf{k}\alpha}. \tag{3}$$

Here, the operator $c^\dagger_{\mathbf{k}\alpha}$ creates an electron with momentum $\mathbf{k}$ and spin $\alpha$ at band $c$. The centers of the two bands are displaced from each other by the AFM ordering vector $\mathbf{Q} = (\pi,\pi)$, and the dispersions are given by

$$\begin{aligned} \varepsilon_{c,\mathbf{k}} &= \mu - 2(t+\delta)\cos k_x - 2(t-\delta)\cos k_y, \\ \varepsilon_{d,\mathbf{k}+\mathbf{Q}} &= -\mu + 2(t-\delta)\cos k_x + 2(t+\delta)\cos k_y, \end{aligned} \tag{4}$$

where $t$ is the hopping parameter, $\mu$ is the chemical potential, and momentum is measured in units of the inverse lattice constant $1/a$. Note that this model is symmetric under the combination of a $\pi/2$ rotation, a particle-hole transformation, and the exchange of the two bands. Hereafter, we set $\mu = t$. By changing the parameter $\delta$, the band dispersions interpolate between two closed nearly nested Fermi pockets ($\delta < t/4$) and two open Fermi surfaces ($\delta > t/4$); see Fig. 2. For $\delta = t/4$, the band dispersion has a saddle point at the Fermi level, implying the existence of a Van Hove singularity, which is characterized by a diverging density of states, $N_f$.

In the spin-fermion model the electrons interact with each other only via the exchange of magnetic fluctuations. As a result, the interaction action is given by

$$S_{\text{int}} = \lambda \sum_j \int_\tau \mathbf{M}_j e^{i\mathbf{Q}\cdot\mathbf{x}_j} \cdot (c^\dagger_{j,\alpha} \boldsymbol{\sigma}_{\alpha\beta} d_{j,\beta} + \text{H.c.}). \tag{5}$$

Here, $j$ denotes lattice sites, $\tau$ is the imaginary time, $\lambda$ is the (Yukawa) coupling constant describing the interaction between electrons and magnetic fluctuations, $\boldsymbol{\sigma}$ are Pauli matrices, and $\mathbf{M}$ is the bosonic field associated with magnetic order with wave vector $\mathbf{Q}$. The spectrum of magnetic fluctuations is determined by the magnetic action, which in turn arises from high-energy electronic degrees of freedom:

$$S_{\text{mag}} = \frac{1}{2} \int_{\mathbf{x},\tau} \left[ \frac{1}{v_s^2} (\partial_\tau \mathbf{M})^2 + (\nabla \mathbf{M})^2 + r M^2 + \frac{u}{2} M^4 \right]. \tag{6}$$

In this expression, $r$ is a tuning parameter that tunes the system through the magnetic quantum critical point, $u = 1/(2t) > 0$ is a parameter penalizing strong amplitude fluctuations, and $v_s = 4t$ is the spin-wave velocity. Note that, in our notation, $\lambda^2$ has dimensions of energy. If $\lambda$ was zero, Eq. (6) would describe a magnetic ordered phase that, at $T = 0$, undergoes a second-order quantum phase transition to a paramagnetic state at $r = r_c$ (see Fig. 1). The coupling to the electrons not only shifts the value of $r_c$, but it also promotes new electronic ordered phases, most notably superconductivity. Additional details about the spin-fermion model are given in Appendix A.

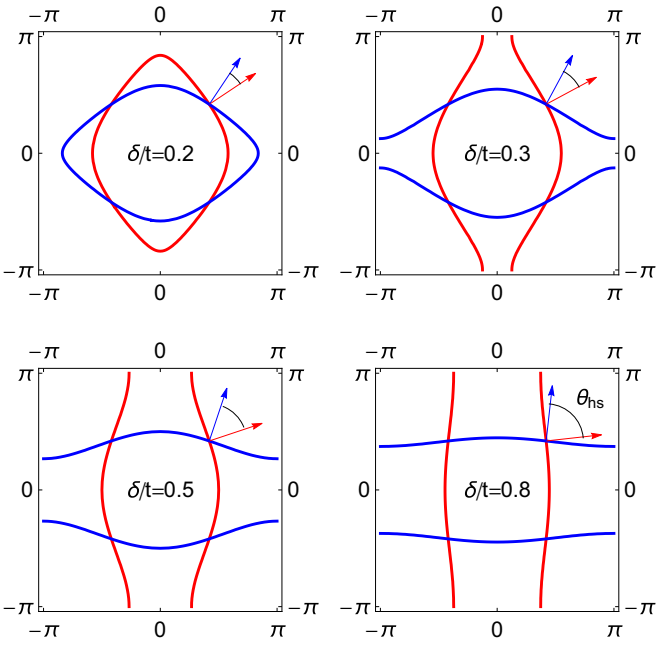


FIG. 2. The two-band spin-fermion model. Fermi surfaces corresponding to the two bands (red and blue curves) in the first Brillouin zone, for different values of $\delta/t$. One of the bands (blue) is displaced by the AFM wave vector $\mathbf{Q} = (\pi,\pi)$, which makes both Fermi surfaces appear concentric. In this representation, a pair of hot spots, defined by $\varepsilon_{c,\mathbf{k}_{\text{hs}}} = \varepsilon_{d,\mathbf{k}_{\text{hs}}+\mathbf{Q}} = 0$, correspond to the points at which the two Fermi surfaces overlap. For the system parameters used here, the hot spots are always along the diagonals of the Brillouin zone. By changing the parameter $\delta/t$, the system interpolates between closed nearly nested Fermi surfaces ($\delta/t < 1/4$) and open Fermi surfaces ($\delta/t > 1/4$), crossing a Van Hove singularity at $\delta/t = 1/4$. The angle $\theta_{\text{hs}}$ between the Fermi velocities of a pair of hot spots (red and blue arrows) increases as function of $\delta/t$ (note that one of the Fermi velocities has been multiplied by $-1$ for clarity purposes).

## III. SIGN-PROBLEM-FREE QUANTUM MONTE CARLO SIMULATIONS

Equations (3), (5), and (6) define the two-band spin-fermion model. Because the total fermionic action $S_0 + S_{\text{int}}$ commutes with an antiunitary operator for every configuration of $\mathbf{M}$, all eigenvalues of the fermionic determinant are complex-conjugate pairs, implying that determinant QMC simulations do not suffer from the sign problem [24]. Here, $S_0$ is the noninteracting action associated with $\mathcal{H}_0$ in Eq. (3). Previous QMC studies have shown conclusively that, in this type of model, the sign-changing SC pairing susceptibility is strongly enhanced near the magnetic QCP [24–26]. Because the system is two-dimensional, at finite temperatures only quasi-long-range SC order is stabilized, which happens below the Berezinskii-Kosterlitz-Thouless (BKT) transition temperature $T_c$. The latter was shown to be maximum very close to the

putative quantum critical point $r = r_c$ [25]. More recently, similar sign-problem-free QMC approaches have been used to study charge fluctuations near an AFM-QCP and the onset of SC near a nematic QCP [26,28–30].

Here, our goal is to establish which band structure parameters determine $T_c$ and $\chi_{\rm pair}$, in order to shed light on the microscopic mechanism by which quantum critical AFM fluctuations promote superconductivity. Our procedure is the following: for a given band dispersion, labeled by $\delta/t$, we first determine the approximate location of the AFM quantum critical point $r_c$ by analyzing both $\langle \mathbf{M}^2 \rangle$ and the Binder cumulant. To save computational time, we consider an easy-plane AFM order parameter, restricting $\mathbf{M}$ to lie in the XY plane. We verify that the system is in the magnetically disordered state and very close to the QCP by computing the renormalized mass term of the magnetic propagator. Note that for the system to be in a quantum critical regime, it is enough that the magnetic mass term be much smaller than $\pi T_c/\gamma$, where $\gamma$ is the Landau damping. As long as this condition is satisfied, even if at $T = 0$ the AFM transition becomes weakly first order, the system's behavior at finite temperatures would still be nearly indistinguishable from a quantum critical one. The static pairing susceptibility in the sign-changing SC channel, $\chi_{\rm pair}$, is obtained by direct computation of the pair correlation function, while the superfluid density $\rho_s$ is obtained from the current-current correlation function. We study square lattices of sizes $L = 8$, $L = 10$, $L = 12$, and $L = 14$. Spurious finite-size effects are diminished by threading a fictitious magnetic flux quantum through the system. Technical details of the QMC implementation are similar to those in Ref. [25], and are summarized in Appendix B.

For each system size $L$, we associate a transition temperature $T_c(L)$ to the temperature at which the BKT condition is met, $\rho_s = 2T_c/\pi$. In Fig. 3, we show the behavior of $T_c(L)$ at the AFM-QCP as function of the parameter $\delta/t$ introduced in Eq. (4) for a moderately strong interaction parameter $\lambda^2 = 8t$. For most band dispersion parameters, $T_c(L)$ of the two largest system sizes are coincident within the QMC statistical error bars. In these cases, our best estimate for the thermodynamic value of $T_c \equiv T_c(L \to \infty)$ is the value corresponding to the largest system size, $T_c(L_{\rm max})$ (filled symbols in the figure). For the band dispersion parameters in which $T_c$ does not seem to fully converge with system size, namely $\delta/t = 0.6$ and $\delta/t = 0.8$, $T_c(L_{\rm max})$ should be understood as an upper bound on $T_c$. In these cases, we also provide a lower bound on $T_c$, represented by stars in the figure (see Appendix B for more details of this procedure). Clearly, the finite-size effects seem to affect mostly the band dispersion with $\delta/t = 0.8$, which has a more pronounced one-dimensional character, as shown in Fig. 2(d). Interestingly, analytical studies of the spin-fermion model suggested a strong competition between SC and charge order for quasi-one-dimensional band dispersions [12,13]. Whether this is related to the stronger finite-size effects observed for $\delta/t = 0.8$ is an interesting topic for future investigation.

Surprisingly, Fig. 3 reveals that $T_c$ is not sensitive to the noninteracting density of states $N_f$, which diverges at the Van Hove singularity at $\delta/t = 0.25$, as shown in the same figure (as shown in Appendix B, even for our finite systems, $N_f$ is also peaked at the Van Hove singularity). Instead, we find that $T_c$ increases linearly with $\sin\theta_{\rm hs}$, where $\theta_{\rm hs}$ is the angle between the noninteracting Fermi velocities of a hot-spot pair (see Fig. 2). In contrast to $N_f$, which varies nonmonotonically as function of $\delta/t$, $\sin\theta_{\rm hs}$ changes monotonically according to $\sin\theta_{\rm hs} = \frac{2(\delta/t)}{1+(\delta/t)^2}$.

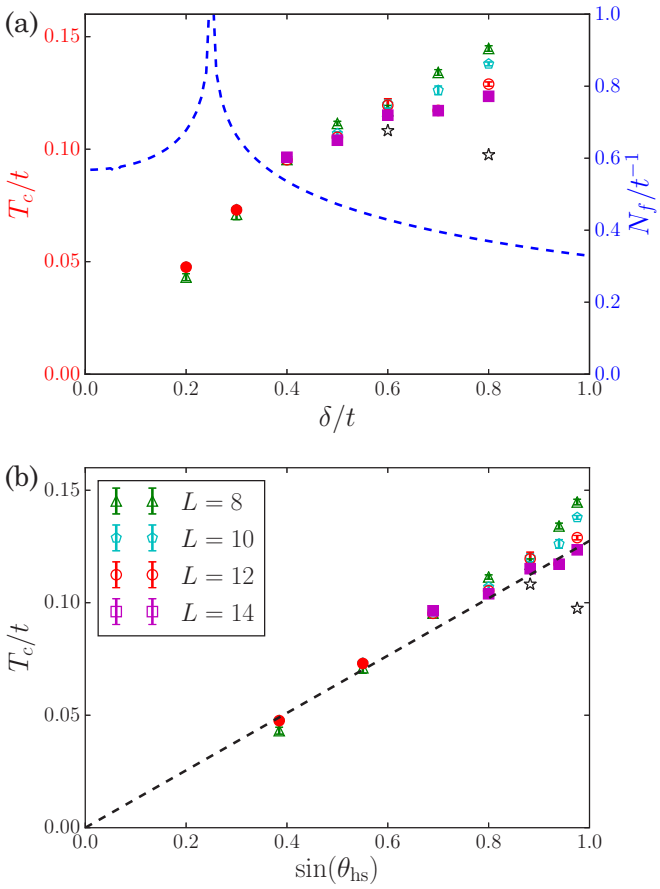


FIG. 3. The superconducting transition temperature $T_c$ at the QCP for different band dispersion parameters. (a) The QMC results for $T_c$ and the calculated density of states $N_f$ (calculated directly from the band dispersions) as function of the band dispersion parameter $\delta/t$ (see Fig. 2). We associate a transition temperature $T_c(L)$ with the temperature at which the BKT condition is met for a system of size $L$, and denote $T_c(L_{\rm max})$ by filled symbols. Analysis of finite-size effects reveals that for most values of $\delta/t$, $T_c(L_{\rm max})$ is a very good estimate for the thermodynamic-limit value $T_c$. For the systems in which $T_c(L)$ does not fully converge, namely $\delta/t = 0.6$ and $\delta/t = 0.8$, $T_c(L_{\rm max})$ are upper bound values for $T_c$, whereas the stars are lower bound values on $T_c$. Note the enhanced $N_f$ at the Van Hove singularity point $\delta/t = 1/4$. (b) The linear relationship between $T_c$ and $\sin\theta_{\rm hs}$, where $\theta_{\rm hs}$ is the angle between the two Fermi velocities of a pair of hot spots, calculated directly from the band dispersions.

The results shown in Fig. 3 imply that the SC transition is rather insensitive to what happens across the entire Fermi surface, but very sensitive to the properties of the hot spots. To further investigate the SC properties of the system, in Fig. 4 we plot the temperature-dependent inverse pairing susceptibility $\chi^{-1}_{\rm pair}(T)$ for all band dispersions at their respective QCPs. We find that, for a rather wide temperature range, the normalized susceptibilities $\chi^{-1}_{\rm pair}(T)/\chi^{-1}_{\rm pair}(3T_c)$ plotted as function of $T/T_c$ collapse onto a single curve, for all values of $\delta/t$ and of $L$. As a result, it follows that the pairing susceptibility must be of the

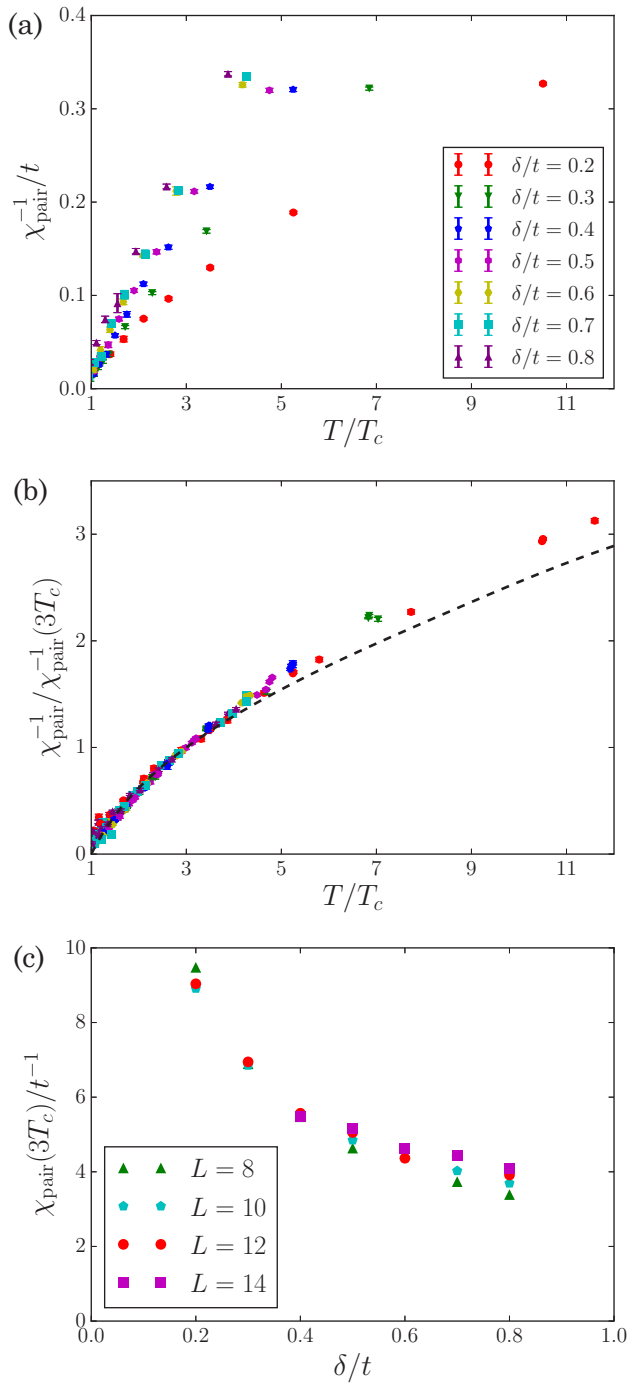


FIG. 4. Universal temperature dependence of the pairing susceptibility $\chi_{\rm pair}$ at the QCP. (a) Temperature dependence of $\chi^{-1}_{\rm pair}$ extracted from QMC simulations for all band dispersion parameters $\delta/t$. The system size is $L = 12$. (b) Collapse of the scaled $\chi^{-1}_{\rm pair}(T)/\chi^{-1}_{\rm pair}(3T_c)$ as function of $T/T_c$ for all values of $\delta/t$ and all system sizes $L$. For each value of $L$, we used the corresponding $T_c(L)$. The black dashed curve is the analytical function $f^{\rm (hs)}_{\rm pair}(T/T_c)/f^{\rm (hs)}_{\rm pair}(3)$ obtained from the hot-spots Eliashberg approximation of the spin-fermion model. (c) The behavior of the QMC-extracted prefactor $A_{\rm pair} \propto \chi_{\rm pair}(3T_c)$ of Eq. (2) as function of $\delta/t$.

form of Eq. (2). While the constant $A_{\rm pair}$, which determines the overall amplitude of the SC fluctuations, depends weakly on $\delta/t$ (see Fig. 4), the function $f_{\rm pair}(T/T_c)$, which determines the temperature dependence of the SC fluctuations, is universal and independent of the band dispersion. Therefore, these results imply that for a wide range of temperatures, the SC fluctuation spectrum is determined by the same energy scale that determines $T_c$—which, according to the analysis in Fig. 3, is related to the hot-spots properties.

## IV. COMPARISON WITH THE HOT-SPOTS ELIASHBERG ANALYTICAL APPROXIMATION

To gain a deeper understanding of the origin of our QMC results, we analytically solve the spin-fermion model within the hot-spots Eliashberg approximation introduced in previous works [10,14,31]. Physically, the main assumptions of this approximation are that the magnetic degrees of freedom are much slower than the electronic degrees of freedom, and that the pairing instability arises only from the hot spots (see Appendix A for technical details). Formally, the first assumption can be justified if the number of electronic "flavors" is extended from 1 to $N$, and $N$ is taken to be infinitely large—although recent works have raised important issues on the general validity of a $1/N$ expansion [12,21,22].

One of the main outcomes of the hot-spots Eliashberg approximation is that the dynamics of the quantum magnetic fluctuations ceases to be ballistic and, instead, becomes overdamped due to the decay of spin fluctuations into electron-hole excitations [32]. The strength of this process is encoded in the Landau damping parameter $\gamma \propto v_F^2 \sin\theta_{\rm hs}/\lambda^2$, which depends on the Fermi velocity at the hot spots $v_F$, on the interaction parameter $\lambda$, and on the hot-spot angle $\sin\theta_{\rm hs}$. The latter is nothing but a constraint on the phase space available for the decay of the spin fluctuations into electron-hole pairs. This property already suggests that the dependence of $T_c$ on $\sin\theta_{\rm hs}$ observed in the QMC results must be connected to the Landau damping. Indeed, a full analysis reveals that, at the QCP, the only energy scale in the hot-spots Eliashberg approximation is given by

$$\Lambda_{\rm QCP} \propto \left(\frac{\lambda^2}{v_F}\right)^2 \gamma \propto \lambda^2 \sin\theta_{\rm hs}, \tag{7}$$

which does not depend on the density of states or the Fermi velocity. Consequently, the superconducting transition temperature at the QCP can only depend on this energy scale [14,31], yielding $T_c^{\rm (hs)} = A_c^{\rm (hs)} \lambda^2 \sin\theta_{\rm hs}$, in agreement with the QMC results. We use the superscript (hs) to distinguish the calculated $T_c^{\rm (hs)}$ from the numerically obtained $T_c$. If we plug in the bare value of the interaction parameter on the hot-spots Eliashberg approximation, we obtain $T_c^{\rm (hs)}/t = 0.14 \sin\theta_{\rm hs}$, which is very close to the linear fitting in Fig. 3, $T_c^{\rm (hs)}/t = 0.13 \sin\theta_{\rm hs}$. However, in comparing $T_c^{\rm (hs)}$ with our QMC results, it is important to recognize that the BKT physics is absent in the hot-spots Eliashberg approximation. Of course, if the phase fluctuations responsible for the suppression of $T_c^{\rm (hs)}$ are only weakly sensitive to the band structure parameters [33], then the Eliashberg transition temperature $T_c^{\rm (hs)}$ and the BKT transition temperature $T_c$ should be simply related by a constant $\alpha$, $T_c = \alpha T_c^{\rm (hs)}$. The fact that $T_c$ scales linearly with $\sin\theta_{\rm hs}$ in our QMC simulations suggests that this is indeed the case.

We can also compute the pairing susceptibility $\chi^{\rm (hs)}_{\rm pair}(T)$ within the hot-spots Eliashberg approximation. At the QCP, we

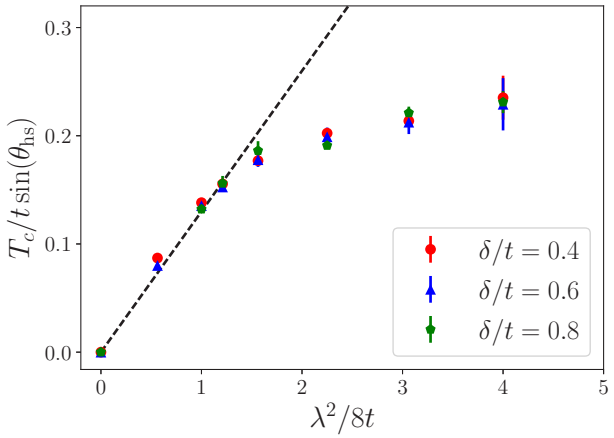


FIG. 5. Dependence of the superconducting transition temperature on the interaction strength. For three values of the band dispersion parameter $\delta/t$, we show the QMC results for $T_c$, in units of the hopping parameter $t$ and normalized by the corresponding value of $\sin\theta_{hs}$, as function of the squared coupling constant $\lambda^2$ (in units of $8t$) describing how strong the electrons interact with AFM fluctuations. The system size is $L = 12$. The dashed line, which denotes a $\lambda^2$ dependence, has the same slope as in Fig. 3(b), and is expected from the analytical hot-spots Eliashberg solution of the spin-fermion model. The absence of the data point corresponding to $\delta/t = 0.8$ and $\lambda^2 = 4.5t$ is because $T_c$ did not converge as a function of the system size for these parameters.

obtain an expression of the form of Eq. (2), with the universal function $f_{\text{pair}}^{(\text{hs})}(T/T_c)$ plotted together with the collapsed QMC points in Fig. 4. The overall agreement between the two curves is evident and, surprisingly, holds over a rather wide temperature range. This confirms our previous conclusion that $f_{\text{pair}}(x)$ arises from hot-spots properties. The fact that the analytical function $f_{\text{pair}}^{(\text{hs})}(T/T_c)$, which is insensitive to BKT physics, captures well the behavior of the QMC-derived function $f_{\text{pair}}(T/T_c)$ suggests that vortex-antivortex fluctuations characteristic of the BKT transition do not play a major role in our QMC simulations. Indeed, for all system sizes studied, $\chi_{\text{pair}}(T)$ does not show any indication of an exponential temperature dependence near $T_c$.

An important prediction of the hot-spots Eliashberg approximation is that $T_c$ increases not only with $\sin\theta_{hs}$ but also with $\lambda^2$. As a result, if the hot-spots Eliashberg approximation is correct, $T_c$ would not be bounded and could increase indefinitely as function of the interaction parameter $\lambda$. To verify this property, we chose three band dispersion parameters and obtained $T_c$ for several values of $\lambda$. As shown in Fig. 5, we find a reasonable scaling of $T_c/\sin\theta_{hs}$ with $\lambda^2$ for moderately large values of the interaction parameter, i.e., $\lambda^2$ of the order of the bandwidth $8t$. The slope of this line is the same as that in Fig. 3(b). Note that for $\lambda = 0$, we have a system of noninteracting electrons with $\chi_{\text{pair}} = 2N_f \ln(\frac{\Lambda}{T})$, implying that $T_c = 0$. More interestingly, for $\frac{\lambda^2}{8t} \gtrsim 2$, we start observing strong deviations from the $\lambda^2$ behavior, signaling the failure of the hot-spots Eliashberg approximation. Furthermore, in this regime, $T_c$ increases very mildly and seems to saturate.

To shed light on this behavior, we note that a key approximation of the hot-spots Eliashberg approach is that the momentum associated with the hot-spots typical energy scale—also called the hot-spots width, $\delta q_{hs} \sim a^{-1}\sqrt{T_c/\gamma}$—is small compared to the Fermi momentum $q_F \sim 1/a$. However, because both $T_c$ and $\gamma^{-1}$ increase with $\lambda^2$, the hot-spots width $\delta q_{hs}$ also increases with $\lambda^2$, and eventually becomes comparable to $q_F$ for large enough values of $\lambda$. In this situation, the whole Fermi surface becomes hot and effectively behaves as a "large hot spot." In this case, as shown in Appendix B, the system still has a single energy scale at the QCP, but instead of Eq. (7) it is given by

$$\tilde{\Lambda}_{\text{QCP}} \propto p_0\left(\frac{\lambda^2}{v_F}\right)\gamma \propto p_0 v_F \sin\theta_{hs}, \tag{8}$$

where $p_0$ is a momentum scale associated with the size of the Fermi surface, and therefore is not a hot-spot property. Thus, in this limit, $T_c^{(\text{hs})}$ becomes independent of $\lambda$ and saturates. A similar behavior was found in Ref. [27] for the one-band spin-fermion model. Therefore, we can attribute the near saturation of $T_c$ observed in our QMC results to a crossover from pairing dominated by the hot spots to pairing dominated by the entire Fermi surface. Naively, in the latter case, one would expect $T_c$ to be more sensitive to the Van Hove singularity. Interestingly, our QMC results for $\frac{\lambda^2}{8t} = 4$ do not reveal a sharp enhancement near $\delta = t/4$ (see Appendix B). One possible reason for this behavior is that the Fermi surface properties become less important when interactions become too strong. While a detailed analysis is beyond the scope of this paper [34], future analytical studies of the spin-fermion model near a Van Hove singularity could shed light on this behavior.

## V. CONCLUDING REMARKS

In summary, we showed that within the spin-fermion model the SC properties near an AFM quantum critical point, including both the transition temperature $T_c$ and the temperature-dependent pairing susceptibility $\chi_{\text{pair}}$, are dominated by the properties of the hot spots, while being rather insensitive to the global properties of the Fermi surface. More specifically, the functional dependencies of $T_c$ and $\chi_{\text{pair}}$ inferred from our QMC results, given by Eqs. (1) and (2), are very well captured by an approximate analytical solution of the spin-fermion model that focuses on the impact of the Landau damping on the pairing interaction. In other words, the hot-spots Eliashberg approach provides an excellent approximate solution to the spin-fermion model, which presumably should hold also for systems with different types of band dispersions beyond the rather artificial two-band case. It is surprising that such an approximation works well even for moderately large values of the interaction $\lambda^2$ between the AFM fluctuations and the low-energy electronic states. However, our combined QMC-analytical analysis also reveals that when $\lambda^2$ becomes larger than the electronic bandwidth, the hot-spots approximation fails. Interestingly, at this crossover from hot-spots-dominated pairing to Fermi-surface-dominated pairing, $T_c$ seems to start saturating, signaling that the maximum possible $T_c$ value for this model has been achieved.

Our results have important implications for the understanding of quantum critical pairing in general. On the one hand, by establishing that the properties of the hot spots govern the SC properties of the low-energy spin-fermion model, it offers

important insights into which of the many system parameters should be changed to optimize $T_c$ in an ideal system. For instance, it becomes clear that systems with nearly nested Fermi surfaces, where $\sin\theta_{\rm hs}$ is small, despite having an abundance of low-energy magnetic fluctuations, have a much smaller transition temperature than systems with non-nested Fermi surfaces, where $\sin\theta_{\rm hs}$ is larger. Conversely, our results establish robust and well-defined benchmarks that allow one to assess whether the SC state obtained in other microscopic models—or even the superconducting state observed in actual materials—falls within the "universality class" of the low-energy spin-fermion model. Two such benchmarks, for instance, are the linear dependence of $T_c$ on $\sin\theta_{\rm hs}$ and the saturation of $T_c$ for large interactions. Large-cluster DMFT simulations of the Hubbard model [18–20] may be able to test these benchmarks and elucidate whether the superconducting properties of the Hubbard model are determined by hot-spots properties or whether they depend on physics beyond the spin-fermion model. On the experimental front, the most promising material candidates that show signatures of AFM quantum criticality near optimal doping are electron-doped cuprates and isovalent-doped pnictides. As for hole-doped cuprates, although they do have a putative AFM quantum critical point, they also display phenomena that have yet to be observed in QMC simulations of the spin-fermion model, such as additional intertwined ordered phases [35] and a transition from small to large Fermi surface without an obvious accompanying order [36]. One interesting possibility is to investigate how pressure affects $T_c$ in these compounds, and correlate these changes with the pressure-induced modifications of the hot-spots properties.

## ACKNOWLEDGMENTS

We thank A. Chubukov, J. Kang, S. Kivelson, S. Lederer, and J. Schmalian for useful discussions. X.W. and R.M.F. were supported by the US Department of Energy, Office of Science, Basic Energy Sciences, under Award No. DE-SC0012336. R.M.F. and X.W. thank the Minnesota Supercomputing Institute (MSI) at the University of Minnesota, where part of the numerical computations was performed. R.M.F. also acknowledges partial support from the Research Corporation for Science Advancement via the Cottrell Scholar Award, and X.W. acknowledges support from the Doctoral Dissertation Fellowship offered by the University of Minnesota. E.B. was supported by the Israel Science Foundation under Grant No. 1291/12, by the US-Israel BSF under Grant No. 2014209, by a Marie Curie career reintegration grant, and by an Alon fellowship. R.M.F. and E.B. are grateful for the hospitality of the Aspen Center for Physics, where part of this work was developed. The Aspen Center for Physics is supported by National Science Foundation Grant No. PHY-1066293.

## APPENDIX A: SPIN-FERMION MODEL: HOT-SPOTS ELIASHBERG APPROXIMATION

### 1. Calculation of $T_c$

The hot-spots Eliashberg approximation consists basically of three steps (see for instance Refs. [10,14]): (i) the bosonic self-energy $\Pi(\mathbf{q},\omega_n)$ is computed within one loop; (ii) the normal and anomalous parts of the fermionic self-energy $\Sigma(\mathbf{q},\omega_n)$ are solved self-consistently within one loop, without vertex corrections; (iii) the resulting gap equations are solved only at the hot spots. In this approximation, the electronic band dispersions are linearized in the vicinities of the hot spots, $\varepsilon_{i\mathbf{k}} \approx \mathbf{v}_{F,i}\cdot(\mathbf{k}-\mathbf{k}_{\rm hs})$. For the specific band dispersions of our model, because the hot spots are always along the diagonal $|k_x| = |k_y|$, we have $|\mathbf{v}_{F,i}| = v_F$ for all hot spots, with

$$v_F = 2t\sqrt{2\left[1-\left(\frac{\mu}{4t}\right)^2\right]\left[\left(\frac{\delta}{t}\right)^2+1\right]}. \tag{A1}$$

Another quantity that also depends on the band dispersion parameter $\delta$ is the angle between the Fermi velocities of a hot-spot pair:

$$\sin\theta_{\rm hs} = \frac{2(\delta/t)}{1+(\delta/t)^2}. \tag{A2}$$

Note that the angle is always defined such that $\sin\theta_{\rm hs} > 0$. After computing the one-loop bosonic self-energy, we find the renormalized propagator:

$$\chi^{-1}(\mathbf{q},i\Omega_n) = \tilde{r} + \mathbf{q}^2a^2 + \frac{|\Omega_n|}{\gamma}, \tag{A3}$$

where $\tilde{r} = r - \Pi(0,0)$ is the renormalized mass term, and the Landau damping coefficient is given by

$$\gamma = \frac{\pi v_F^2 \sin\theta_{\rm hs}}{\lambda^2 N}. \tag{A4}$$

Here, $\lambda$ is the Yukawa coupling constant, and $N$ is the number of hot-spots pairs, which in our model is $N = 4$. To compute the one-loop self-consistent self-energy, it is convenient to work on Nambu space, defined by the spinors $\psi^\dagger_{c,\mathbf{k}} \equiv (c^\dagger_{\mathbf{k}\uparrow}, c_{-\mathbf{k}\downarrow})$, and $\psi^\dagger_{2,\mathbf{k}} \equiv (d^\dagger_{\mathbf{k}+\mathbf{Q}\uparrow}, d_{-\mathbf{k}-\mathbf{Q}\downarrow})$. The self-energy is then given by

$$\hat{\Sigma}_{c,k} = \frac{n_b\lambda^2}{\beta V}\sum_p \chi(k-p)\hat{G}_{d,p}, \tag{A5}$$

where $n_b = 1,2,3$ for Ising, XY, and Heisenberg spins, respectively. Here, $\beta$ is the inverse temperature, $V = L^2$ is the volume of the system, and $k = (\omega_n,\mathbf{k})$. Hereafter, we will measure all momenta in units of the inverse lattice spacing $1/a$. To proceed, we parametrize the fermionic self-energy as $\hat{\Sigma}_{i,k} = (1-Z_{i,k})i\omega_n\tau_0 + \zeta_{i,\mathbf{k}}\tau_3 + \phi_{i,k}\tau_1$, where $\tau$ are Pauli matrices in Nambu space. The normal components of the self-energy are thus expressed in terms of $Z_{i,k}$ and $\zeta_{i,k}$, whereas the anomalous part, proportional to the superconducting gap, is expressed in terms of $\phi_{i,k}$. From Dyson's equations, we obtain the dressed Green's function:

$$\hat{G}_{i,k} = -\frac{Z_{i,k}i\omega_n + \varepsilon_{i,\mathbf{k}}\tau_3 + \phi_{i,k}\tau_1}{Z^2_{i,k}\omega_n^2 + \varepsilon^2_{i,\mathbf{k}} + \phi^2_{i,k}} \tag{A6}$$

with renormalized $\varepsilon_{i,\mathbf{k}} \to \varepsilon_{i,\mathbf{k}} + \zeta_{i,\mathbf{k}}$. Substitution back into Eq. (A5) and linearizing in $\phi_i$, we find the self-consistent equations

$$(1-Z_{1,k})i\omega_n = -\frac{n_b\lambda^2}{\beta V}\sum_{\omega_m,\mathbf{p}}\chi(\mathbf{k}-\mathbf{p},i\omega_n - i\omega_m) \times\left(\frac{Z_{2,p}i\omega_m}{Z^2_{2,p}\omega_m^2+\varepsilon^2_{2,\mathbf{p}}}\right),$$

$$\phi_{1,k} = -\frac{n_b\lambda^2}{\beta V}\sum_{\omega_m,\mathbf{p}} \chi(\mathbf{k}-\mathbf{p}, i\omega_n - i\omega_m) \times \left(\frac{\phi_{2,p}}{Z_{2,p}^2\omega_m^2 + \varepsilon_{2,\mathbf{p}}^2}\right). \quad \text{(A7)}$$

Analogous equations hold for $Z_{2,k}$ and $\phi_{2,k}$. Note that in the Eliashberg approximation, the bosonic propagator $\chi$ is not calculated self-consistently; i.e., the bosonic self-energy is computed using the noninteracting Green's functions [10].

To proceed, we solve these equations only at the hot spots, and therefore ignore the momentum dependence of the quasiparticle weight $Z$ and of the gap $\phi$. Within the Eliashberg approximation, we only need to consider the variation of the bosonic propagator with respect to the momentum parallel to the Fermi surface, $\chi(\mathbf{q}, i\Omega_n) \approx \chi(q_\parallel, i\Omega_n)$. These key aspects of the hot-spots Eliashberg approximation highlight the fact that the bosonic degrees of freedom are much slower than the fermionic ones. Using these approximations, one can then perform the integration over momentum in the previous expressions by changing coordinates to $(p_\parallel, p_\perp)$, i.e., momenta parallel and perpendicular to the Fermi surface near the hot spots. As a result, $\varepsilon_{i,\mathbf{p}} = v_F p_\perp$, and one obtains

$$Z(\omega_n) = 1 + \frac{n_b\lambda^2 T}{4v_F}\sum_{\omega_m} V_{\text{pair}}(\omega_n - \omega_m)\frac{\text{sgn}(\omega_m)}{\omega_n}, \quad \text{(A8)}$$

$$\phi(\omega_n) = \frac{n_b\lambda^2 T}{4v_F}\sum_{\omega_m} V_{\text{pair}}(\omega_n - \omega_m)\frac{\phi(\omega_m)}{Z(\omega_m)|\omega_m|}. \quad \text{(A9)}$$

To write these expressions, we note that $Z_1 = Z_2$, since the Fermi velocities are the same at both points of the hot-spot pair, and $\phi_1 = -\phi_2$ is the only possible solution to the gap equations. The pairing interaction is given by

$$V_{\text{pair}}(\Omega_n) = \int_{-\frac{p_0}{2}}^{\frac{p_0}{2}} \frac{dp_\parallel}{\pi}\frac{1}{p_\parallel^2 + \tilde{r} + |\Omega_n|/\gamma}, \quad \text{(A10)}$$

where $p_0 \sim O(1)$ is an upper momentum cutoff related to the size of the Fermi surface in the Brillouin zone. This momentum scale is to be compared to the typical "momentum width" of the hot spots, $\delta p_{\text{hs}} = \sqrt{2\pi T_c/\gamma}$, determined by comparing the frequency and momentum dependent terms in Eq. (A3) for the energy scale $\Omega_n = 2\pi T_c$. In the hot-spots Eliashberg approximation, $p_0 \gg \delta p_{\text{hs}}$, and we can replace $p_0 \to \infty$ in the previous expression, yielding

$$V_{\text{pair}}(\Omega_n) = \sqrt{\frac{1}{\tilde{r} + |\Omega_n|/\gamma}}. \quad \text{(A11)}$$

Therefore, the Eliashberg equations become

$$Z(\omega_n) = 1 + \frac{1}{2\pi}\sqrt{\frac{\Lambda_{\text{QCP}}}{T}}\sum_{\omega_m}\frac{1}{\sqrt{|n-m| + \frac{\tilde{r}\gamma}{2\pi T}}}\frac{\text{sgn}(\omega_m)}{n+\frac{1}{2}}, \quad \text{(A12)}$$

$$\phi(\omega_n) = \frac{1}{2\pi}\sqrt{\frac{\Lambda_{\text{QCP}}}{T}}\sum_{\omega_m}\frac{1}{\sqrt{|n-m| + \frac{\tilde{r}\gamma}{2\pi T}}}\frac{\phi(\omega_m)}{Z(\omega_m)|m+\frac{1}{2}|}, \quad \text{(A13)}$$

where we introduced the energy scale:

$$\Lambda_{\text{QCP}} \equiv \left(\frac{n_b\lambda^2}{4v_F}\right)^2\frac{\gamma}{2\pi} = \frac{n_b^2\lambda^2\sin\theta_{\text{hs}}}{32N}. \quad \text{(A14)}$$

The key point is that at the QCP, $\tilde{r} = 0$, and the only energy scale in the problem is given by $\Lambda_{\text{QCP}}$ (a similar behavior is found slightly away from the QCP, as long as $\tilde{r} \ll 2\pi T_c/\gamma$). Therefore, the superconducting transition temperature at the QCP is set by the only energy scale in the problem, i.e., $T_c = \alpha\Lambda_{\text{QCP}}$, where $\alpha$ is a number (no cutoff is necessary, in contrast to the BCS case). According to our numerical solution of the Eliashberg equations, we find $\alpha \approx 0.56$, in agreement with previous calculations [14,31]. Note that, as pointed out in Ref. [14], when $\tilde{r} = 0$, the term $m = n$ in the sum that appears in the determination of $Z(\omega_n)$ is exactly canceled by the term $m = n$ in the sum that appears in the determination of $\phi(\omega_n)$. This is easily seen by defining the pairing gap $\Delta \equiv \phi/Z$, and separating out the $m = n$ term from Eqs. (A12):

$$\left[Z(\omega_n) - \frac{1}{2\pi}\sqrt{\frac{\Lambda_{\text{QCP}}}{T}}\sqrt{\frac{2\pi T}{\tilde{r}\gamma}}\frac{1}{|n+\frac{1}{2}|}\right] = 1 + \frac{1}{2\pi}\sqrt{\frac{\Lambda_{\text{QCP}}}{T}}\sum_{\omega_m\neq\omega_n}\frac{1}{\sqrt{|n-m| + \frac{\tilde{r}\gamma}{2\pi T}}}\frac{\text{sgn}(\omega_m)}{n+\frac{1}{2}}, \quad \text{(A15)}$$

$$\Delta(\omega_n)\left[Z(\omega_n) - \frac{1}{2\pi}\sqrt{\frac{\Lambda_{\text{QCP}}}{T}}\sqrt{\frac{2\pi T}{\tilde{r}\gamma}}\frac{1}{|n+\frac{1}{2}|}\right] = \frac{1}{2\pi}\sqrt{\frac{\Lambda_{\text{QCP}}}{T}}\sum_{\omega_m\neq\omega_n}\frac{1}{\sqrt{|n-m| + \frac{\tilde{r}\gamma}{2\pi T}}}\frac{\Delta(\omega_m)}{|m+\frac{1}{2}|}. \quad \text{(A16)}$$

Therefore the $m = n$ term does not enter into the linearized gap equation, and that there is a finite superconducting transition temperature in the limit $r \to 0$. It is important to note that $\lambda^2/N$ does not necessarily have the same bare value that enters the Hamiltonian in the QMC simulations, since magnetic fluctuations are known to effectively renormalize the interactions. If nevertheless we use the bare values of $\lambda$ and $N$ to estimate $T_c$, i.e., $\lambda^2 = 8t$ and $N = 4$, we would get $T_c/t \approx 0.14\sin\theta_{\text{hs}}$, which is about 10% larger than the BKT superconducting transition temperature obtained from the QMC simulations.

It is also instructive to consider the opposite limit in which the entire Fermi surface becomes hot, i.e., $p_0 \ll \delta p_{\text{hs}}$. This is certainly the case when $2\pi T_c \gg \gamma$; since $T_c, \gamma^{-1} \propto \lambda^2$, this means that this limit is achieved for large values of the Yukawa coupling. In this case, the pairing interaction becomes

$$V_{\text{pair}}(\Omega_n) = \frac{p_0/\pi}{\tilde{r} + |\Omega_n|/\gamma}. \quad \text{(A17)}$$

As a result, at the QCP, $\tilde{r} = 0$, there is still only one energy scale in the Eliashberg equations, now set by

$$\tilde{\Lambda}_{\text{QCP}} \equiv \frac{p_0}{\pi}\left(\frac{n_b\lambda^2}{4v_F}\right)\frac{\gamma}{2\pi} = \frac{n_b p_0 v_F\sin\theta_{\text{hs}}}{8\pi N}. \quad \text{(A18)}$$

The Eliashberg equations become

$$Z(\omega_n) = 1 + \frac{1}{2\pi}\left(\frac{\tilde{\Lambda}_{\rm QCP}}{T}\right)\sum_{\omega_m}\frac{1}{|n-m|+\frac{\tilde{r}\gamma}{2\pi T}}\frac{\mathrm{sgn}(\omega_m)}{n+\frac{1}{2}}, \tag{A19}$$

$$\phi(\omega_n) = \frac{1}{2\pi}\left(\frac{\tilde{\Lambda}_{\rm QCP}}{T}\right)\sum_{\omega_m}\frac{1}{|n-m|+\frac{\tilde{r}\gamma}{2\pi T}}\frac{\phi(\omega_m)}{Z(\omega_m)|m+\frac{1}{2}|}. \tag{A20}$$

Therefore, at $\tilde{r}=0$, $T_c = \tilde{\alpha}\tilde{\Lambda}_{\rm QCP}$ becomes independent of the Yukawa coupling, and may depend on additional properties of the Fermi surface, as indicated by the presence of the momentum scale $p_0$ in $\tilde{\Lambda}_{\rm QCP}$. Note that due to similar arguments described in Eq. (A15), the $n=m$ term does not appear in the linearized gap equation.

### 2. Calculation of the pairing susceptibility

To compute the static pairing susceptibility in the sign-changing gap channel, we first introduce in the Hamiltonian the pairing field $\Delta$:

$$\delta H = -2\Delta\sum_{\mathbf{k}}(c_{\mathbf{k}\uparrow}c_{-\mathbf{k}\downarrow} - d_{\mathbf{k}\uparrow}d_{-\mathbf{k}\downarrow} + \text{H.c.}). \tag{A21}$$

Here the factor of 2 is included so that the definition of the pairing vertex is consistent with that used in the QMC simulations. In Dyson's equation, this term can be incorporated in the self-energy, $\hat{\Sigma}_i \to \hat{\Sigma}_i - 2\Delta\tau_1$. Repeating the same steps as above, the only modification is in the gap equation:

$$\phi(\omega_n) = \frac{n_b\lambda^2 T}{4v_F}\sum_{\omega_m}V_{\rm pair}(\omega_n-\omega_m)\frac{\phi(\omega_m)}{Z(\omega_m)|\omega_m|} + 2\Delta. \tag{A22}$$

We considered the linearized equation because we are interested only in the susceptibility of the disordered state, where $\phi = 0$. Defining $\eta(\omega_n) \equiv \partial\phi(\omega_n)/\partial\Delta$, we obtain a self-consistent equation for $\eta(\omega_n)$:

$$\eta(\omega_n) = \frac{n_b\lambda^2 T}{4v_F}\sum_{\omega_m}V_{\rm pair}(\omega_n-\omega_m)\frac{\eta(\omega_m)}{Z(\omega_m)|\omega_m|} + 2, \tag{A23}$$

$$\eta(\omega_n) = \frac{1}{2\pi}\sqrt{\frac{\Lambda_{\rm QCP}}{T}}\sum_{\omega_m}\frac{1}{\sqrt{|n-m|}}\frac{\eta(\omega_m)}{Z(\omega_m)|m+\frac{1}{2}|} + 2. \tag{A24}$$

Now, the static pairing susceptibility is given by

$$\chi_{\rm pair} \equiv \chi(\mathbf{q}\to 0, i\Omega_n \to 0) = \partial_\Delta\sum_k 2\langle c_{k\uparrow}c_{-k\downarrow} - d_{k\uparrow}d_{-k\downarrow}\rangle, \tag{A25}$$

where $k = (\omega_n, \mathbf{k})$ and $\sum_k = T\sum_n\int\frac{d^2k}{(2\pi)^2}$. Because the mean value is precisely minus the anomalous part of the Green's function, $\phi_{i,k}$, given by Eq. (A8), we obtain

$$\chi_{\rm pair} = 4T\sum_{\omega_n}\int\frac{d^2k}{(2\pi)^2}\frac{\eta(\omega_n)}{Z(\omega_n)^2\omega_n^2+\varepsilon_{\mathbf{k}}^2}. \tag{A26}$$

Note that, for $\lambda = 0$ (noninteracting electrons), we have $Z(\omega_n) = 1$, $\eta(\omega_n) = 2$, and the equation above reduces to the well-known BCS expression

$$\begin{aligned}\chi_{\rm pair} &= 8T\sum_{\omega_n,\mathbf{k}}\frac{1}{\omega_n^2+\varepsilon_{\mathbf{k}}^2}\\ &= 4\sum_{i,k}G_i^{(0)}(k)G_i^{(0)}(-k)\\ &= 2N_f\ln\frac{\Lambda}{T},\end{aligned} \tag{A27}$$

where $N_f = 4\int\frac{\mathrm{d}^2\mathrm{k}}{(2\pi)^2}\delta(\varepsilon_{\mathbf{k}})$ is the total density of states at the Fermi level. The factor of 4 arises due to band and spin degeneracies.

For $\lambda \neq 0$, it is convenient once again to integrate along directions parallel and perpendicular to the Fermi surface, yielding

$$\chi_{\rm pair} = \frac{p_0}{2\pi^2 v_F}\sum_{\omega_n}\frac{\eta(\omega_n)}{Z(\omega_n)|n+\frac{1}{2}|}, \tag{A28}$$

where $p_0$ is the same quantity as defined in the previous section. Because the equations for $\eta(\omega_n)$ and $Z(\omega_n)$, Eqs. (A23) and (A12), depend only on $T/\Lambda_{\rm QCP} \propto T/T_c$, it follows that the susceptibility is of the form $\chi_{\rm pair}(T) = A_{\rm pair}f_{\rm pair}(\frac{T}{T_c})$, where $A_{\rm pair}$ depends on the Fermi surface properties (as signaled by $p_0$ above), but $f_{\rm pair}(\frac{T}{T_c})$ is a universal function.

In computing $\chi_{\rm pair}$ numerically, it is important to keep in mind that as higher temperatures are considered, the effect of the bandwidth becomes more important, as the bandwidth $8t$ provides a natural energy cutoff for the Matsubara sum. Note that this is not an issue for the computation of $T_c$, since $T_c \ll 8t$ always. Because $8t$ is a hard cutoff in real frequency space, to capture its effects in Matsubara frequency space, we follow Ref. [31] and introduce a soft cutoff:

$$\Upsilon(\omega_n) = \frac{1}{\exp\left[(\omega_n - 8t)/\omega_0\right]+1}. \tag{A29}$$

This function appears not only in the Matsubara sum present in $\chi_{\rm pair}$, but also in the self-consistent equation for $\zeta(\omega_n)$ via

$$\begin{aligned}\eta(\omega_n) = 2\Upsilon(\omega_n) &+ \frac{1}{2\pi}\sqrt{\frac{\Lambda_{\rm QCP}}{T}}\\ &\times\left[\sum_{\omega_m}\frac{\Upsilon(\omega_n)\Upsilon(\omega_m)}{\sqrt{|n-m|}}\frac{\eta(\omega_m)}{Z(\omega_m)|m+\frac{1}{2}|}\right].\end{aligned} \tag{A30}$$

For the plot in Fig. 4(b) of the main text, we used $\omega_0 = 1.6t$. Changing this parameter slightly does not affect the main properties of $\chi_{\rm pair}$.

## APPENDIX B: DETERMINANT QUANTUM MONTE CARLO

The technical details of the implementation of the determinant quantum Monte Carlo (QMC) for the two-band spin-fermion model with XY spins are the same as those extensively presented in Ref. [25], co-authored by two of us. As explained in the main text, in this work our goal is to establish the band structure parameters that determine $T_c$

and $\chi_{\rm pair}$. Our procedure is the following: for a given set of parameters, we first determine the approximate location of the AFM quantum critical point $r_c$ and then determine $T_c$ from the condition that the superfluid density $\rho_s$ reaches the BKT value $2T_c/\pi$. The static pairing susceptibility is computed directly. In this appendix, we provide more details on how these three quantities are determined for a given set of parameters $(\delta, L, \lambda^2)$, characterized by the band parameter $\delta/t = 0.2, 0.3, 0.4, 0.5, 0.6, 0.7, 0.8$, the system size $L = 8, 10, 12, 14$, and the squared coupling constant $\lambda^2/t = 8$.

### 1. Antiferromagnetic quantum critical point (AFM-QCP)

The AFM-QCP is reached by tuning the bare mass term of the magnetic propagator to $r = r_c$; see Eq. (6) of the main text. Determining the precise location of the QCP is a very difficult task, not only due to the BKT character of the AFM transition at finite temperatures (since we are dealing with XY spins), but also because once superconductivity sets in, it competes with AFM order and shifts the location of the QCP from $r_c$ to $\bar{r}_c < r_c$. This last behavior was indeed observed in the previous QMC studies of Ref. [25]. However, for our purposes, it is not necessary to precisely determine the position $r_c$ of the QCP. As explained in the previous section, the onset of superconductivity within the hot-spots Eliashberg approximation of the spin-fermion model depends on two parameters, $\Lambda_{\rm QCP} \propto \lambda^2 \sin\theta_{\rm hs}$, and the renormalized mass of the magnetic propagator, $\tilde{r}$; see for instance Eqs. (A11) and (A12). Thus, as long as $\tilde{r} \ll 2\pi T_c/\gamma$, the superconducting properties of the system are effectively the same as those at the QCP. Therefore, to probe quantum critical pairing, we search for a value of $r$ sufficiently close to $r_c$ such that $\tilde{r}$ is very small, but nonzero, since we must ensure that the system is not in the AFM ordered phase.

For this purpose, we first define the uniform magnetization:

$$\bar{\mathbf{M}} \equiv \frac{1}{\beta L^2} \sum_{\mathbf{r}} \int d\tau\, \mathbf{M}(\mathbf{r},\tau). \tag{B1}$$

To obtain a good estimate of $r_c$, we extract from the QMC simulations both the Binder cumulant,

$$\mathcal{B} = 1 - \frac{\langle (\bar{\mathbf{M}}^2)^2 \rangle}{2\langle \bar{\mathbf{M}}^2 \rangle^2}, \tag{B2}$$

and the static spin susceptibility,

$$\chi_M \equiv \frac{1}{\beta L^2} \left\langle \sum_{\mathbf{r},\tau} \sum_{\mathbf{r}',\tau'} \mathbf{M}(\mathbf{r},\tau) \cdot \mathbf{M}(\mathbf{r}',\tau') \right\rangle = \beta L^2 \langle \bar{\mathbf{M}}^2 \rangle. \tag{B3}$$

Here, $\langle \cdots \rangle$ denotes thermal averaging. For XY spins deep in the ordered phase, $\mathcal{B} = \frac{1}{2}$, whereas $\mathcal{B} = 0$ deep in the disordered phase. Similarly, in the ordered phase, $\chi_M$ scales with $\beta L^{2-\eta}$, where $\eta$ changes continuously as function of $r$ and $T$, approaching $\eta = 0$ deep in the ordered phase. Therefore, at any finite temperature, a rough estimate for the AFM transition is given by the value of $r$ in which $\chi_M/(\beta L^2)$ shows a kink and $\mathcal{B}$ changes sharply from 0 to 1/2. In Fig. 6, we show the behavior of these two quantities, plotted as function of $r$ for different fixed temperatures, for the set of parameters $(\delta/t, L, \lambda^2/t) = (0.6, 12, 8)$. On the scale shown in this figure, both $\mathcal{B}$ and $\chi_M/(\beta L^2)$ are nearly temperature independent at low temperatures (but still above $T_c$), therefore providing an estimate for $r_c$.

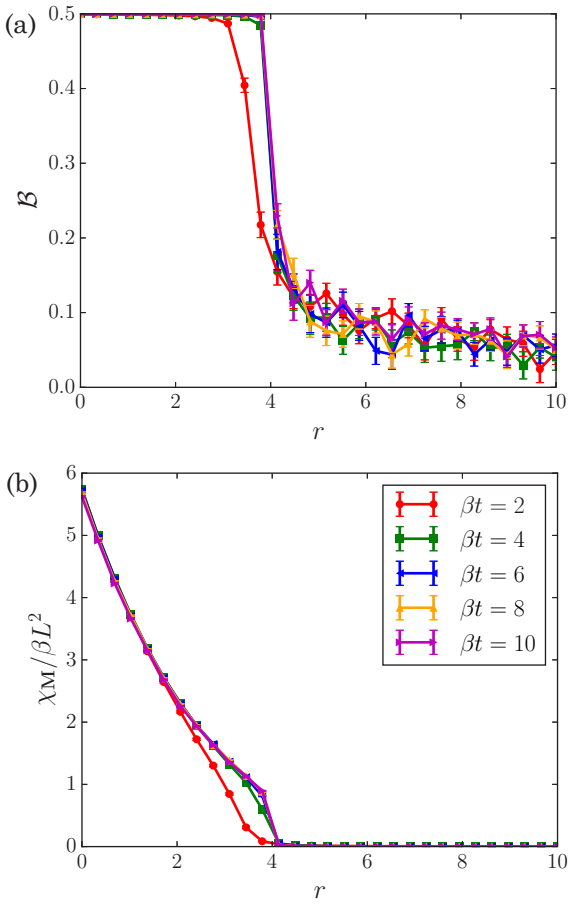


FIG. 6. Binder cumulant $\mathcal{B}$ (a) and static spin susceptibility $\chi_M$ (b) as a function of $r$ for various inverse temperatures. The set of parameters used here is $(\delta/t, L, \lambda^2/t) = (0.6, 12, 8)$. The inverse temperature $\beta$ is in units of $1/t$.

Next, to improve our estimate of $r_c$, we compute the $r$ dependence of the mass of the bosonic propagator at low temperatures, $\tilde{r} \equiv \chi_M^{-1}(\mathbf{q} = 0, i\Omega_n = 0)$, as shown in Fig. 7(a). The estimated $r_c$ corresponds to the $r$ value that has the smallest $\tilde{r}$, before however it reaches zero, since we want to study the system in the nonmagnetically ordered state.

In the same figure we also present the frequency and momentum dependencies of $\chi_M^{-1}(\mathbf{q}, i\Omega_n)$. In agreement with a recent study by some of us [32], $\chi_M^{-1}(\mathbf{q} = 0, i\Omega_n)$ shows a rather linear dependence on the Matsubara frequency, indicating the presence of Landau damping, which in turn plays a key role in the hot-spots Eliashberg approximation; see Eq. (A3). Similarly, $\chi_M^{-1}(\mathbf{q}, i\Omega_n = 0)$ is consistent with a $q^2$ behavior for small momentum.

### 2. Pairing susceptibility and superfluid density

The static pairing susceptibility is defined as

$$\chi_{\rm pair}^{(a)} \equiv \frac{1}{\beta L^2} \sum_{\mathbf{r},\mathbf{r}'} \int_{\tau,\tau'} \langle \Gamma_a(\mathbf{r},\tau) \Gamma_a^{\dagger}(\mathbf{r}',\tau') \rangle, \tag{B4}$$

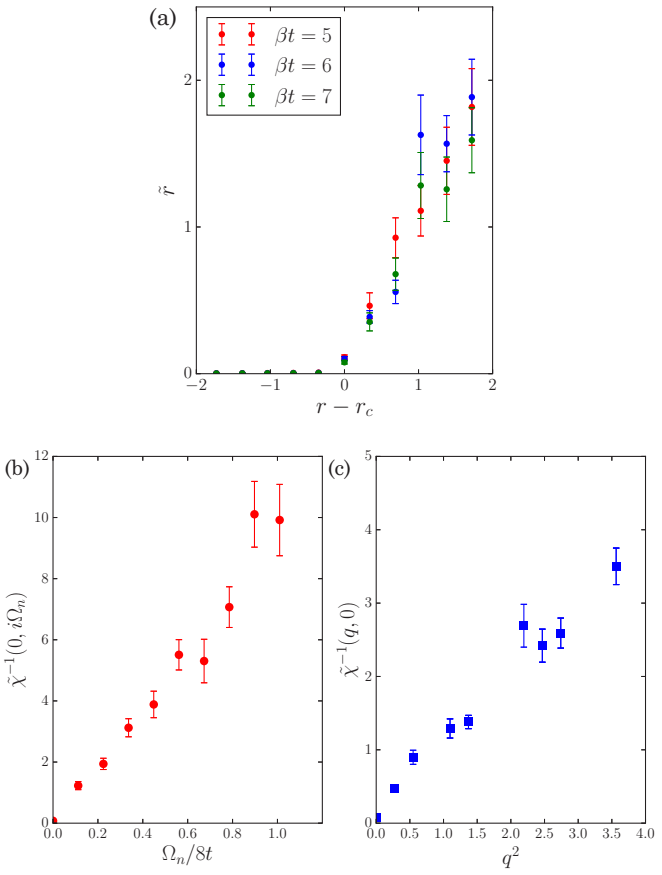


FIG. 7. Panel (a) shows the renormalized mass term of the magnetic propagator, $\tilde{r}$, as function of $r_c$. The set of parameters used here is $(\delta/t,\ L,\ \lambda^2/t) = (0.6,\ 12,\ 8)$. The inverse renormalized magnetic propagator $\tilde{\chi}^{-1}(\mathbf{q}, i\Omega_n)$ at $r = r_c$ is plotted as function of $\Omega_n$ for $\mathbf{q} = 0$ (b) and as function of $q$ for $\Omega_n = 0$ (c). In (b) and (c), the inverse temperature is $\beta = 7/t$.

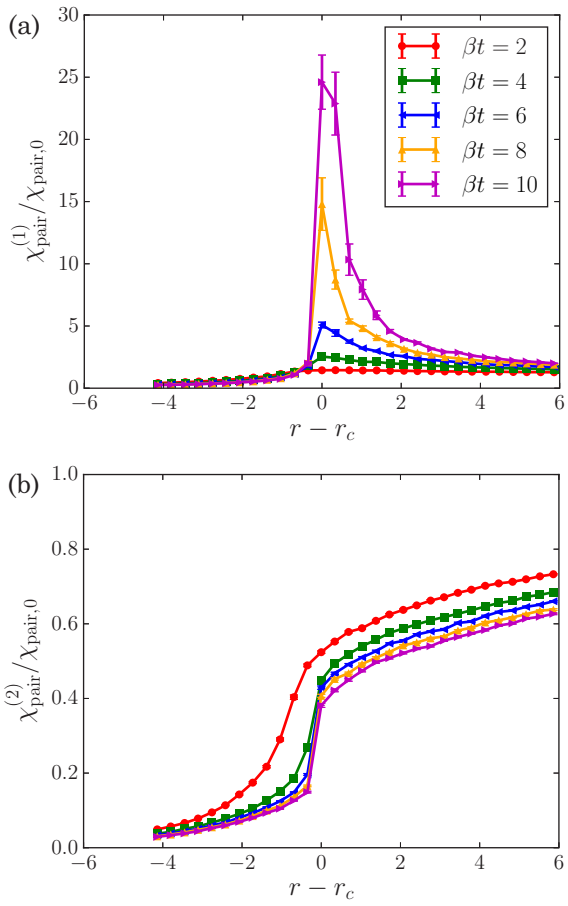


FIG. 8. Static pairing susceptibility $\chi^{(a)}_{\rm pair}$ in the sign-changing gap channel [$a = 1$; panel (a)] and in the in the sign-preserving gap channel [$a = 2$; panel (b)] as function of the distance to the QCP at $r = r_c$. The inverse temperature $\beta$ is in units of $1/t$ and the susceptibilities are normalized by the noninteracting susceptibility $\chi_{\rm pair,0}$ obtained by setting $\lambda = 0$. The set of parameters used here is $(\delta/t,\ L,\ \lambda^2/t) = (0.6,\ 12,\ 8)$.

where

$$\Gamma_a(\mathbf{r},\tau) \equiv i\sigma^y_{\alpha\beta}[c_\alpha(\mathbf{r},\tau)c_\beta(\mathbf{r},\tau) + (-1)^a d_\alpha(\mathbf{r},\tau)d_\beta(\mathbf{r},\tau)] \tag{B5}$$

is the pairing field associated with the sign-changing gap function ($a = 1$) or with the sign-preserving gap function ($a = 2$). $\sigma_y$ is the Pauli matrix in spin space. In Fig. 8, we plot both pairing susceptibilities, in units of the noninteracting susceptibility $\chi_{\rm pair,0}$, as a function of $r$ and as a function of temperature for the set of parameters $(\delta/t,\ L,\ \lambda^2/t) = (0.6,\ 12,\ 8)$. Compared with Fig. 6, it is clear that while $\chi^{(1)}_{\rm pair}/\chi_{\rm pair,0}$ is strongly peaked at $r = r_c$, $\chi^{(2)}_{\rm pair}/\chi_{\rm pair,0}$ is always smaller than 1, implying that there is no enhancement in the sign-preserving channel.

Because the system is two-dimensional, the superconducting phase transition is of the BKT type. Therefore, to determine $T_c$, we search for the temperature where the BKT condition is satisfied:

$$\rho_s(T_c) = \frac{2}{\pi}T_c,$$

where $\rho_s$ is the superfluid density. As explained in Ref. [25], the latter can be extracted from our QMC simulations via the current-current correlation function $\Lambda_{ij}$ according to $\rho_s \equiv \lim_{L\to\infty}\rho_s(L)$, with

$$\rho_s(L) = \frac{1}{8}\sum_{a=x,y}\left\langle \Lambda_{aa}\left(q_a = \frac{2\pi}{L}, q_{\bar{a}} = 0, i\Omega_n = 0\right)\right\rangle \tag{B6}$$

$$-\frac{1}{8}\sum_{a=x,y}\left\langle \Lambda_{aa}\left(q_a = 0, q_{\bar{a}} = \frac{2\pi}{L}, i\Omega_n = 0\right)\right\rangle, \tag{B7}$$

where $\bar{a} = y,x$ when $a = x,y$ and

$$\Lambda_{ij}(\mathbf{r},\tau) \equiv \frac{1}{\beta L^2}\left\langle \int d\tau_1 \sum_{\mathbf{r}_1} j_i(\mathbf{r}+\mathbf{r}_1, \tau+\tau_1) j_j(\mathbf{r}_1,\tau_1)\right\rangle, \tag{B8}$$

with $j_i$ denoting the standard current operator. Note that the model studied here is symmetric under the combination of a $\pi/2$ rotation, a particle-hole transformation, and the exchange of the two bands, implying $\Lambda_{xx}(\mathbf{r},\tau) = \Lambda_{yy}(\tilde{\mathbf{r}},\tau)$, where $\mathbf{r}$ and $\tilde{\mathbf{r}}$ are related by a $\pi/2$ rotation. Figure 9 shows $\rho_s$ for various system sizes for the band dispersion $\delta/t = 0.6$ and

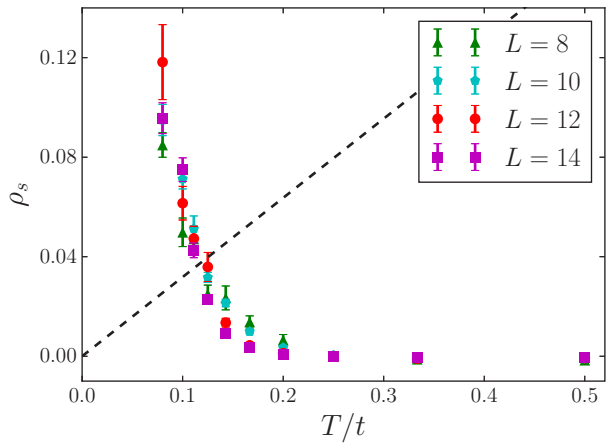


FIG. 9. Superfluid density $\rho_s(L,T)$ as function of temperature $T$ for the band dispersion $\delta/t = 0.6$ and coupling constant $\lambda^2 = 8t$ for various system sizes $L$. The BKT transition temperature for each system size is determined by the condition $\rho_s(L,T_c) = \frac{2}{\pi}T_c$.

the interaction parameter $\lambda^2 = 8t$. The estimated transition temperature $T_c(L)$ for each system of size $L$ is determined as the intersection between the interpolated curve of $\rho_s(L,T)$ and $\frac{2}{\pi}T$. The error bars in $\rho_s$ arising from the QMC sampling are used to estimate the error bars of $T_c$ in the following way: besides the interpolation curve passing through the average values of $\rho_s$, we also determine two additional interpolation curves passing through the top and the bottom of each error bar

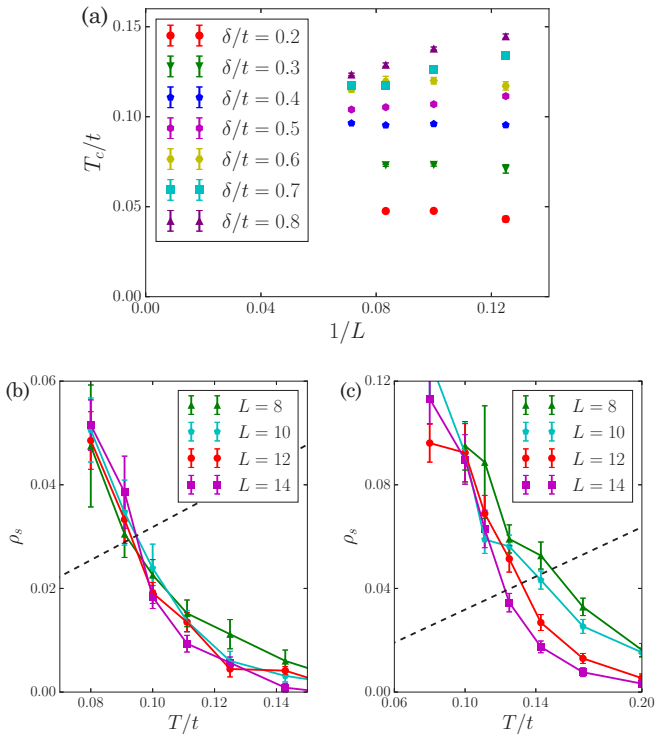


FIG. 10. (a) The QMC extracted $T_c(L)$ as function of the inverse system size $1/L$ for all band dispersion parameters $\delta/t$. Interpolated $\rho_S(T)$ curve for $\delta/t = 0.4$ (b) and for $\delta/t = 0.8$ (c).

related to $\rho_s$. The error bars in $T_c$ are estimated by determining when these two additional curves cross $\frac{2}{\pi}T$.

### 3. Thermodynamic limit of the BKT transition temperature

To estimate the thermodynamic value of the BKT transition, we first plot the extracted $T_c(L)$ as a function of $1/L$ in Fig. 10(a). For most of the values of $\delta/t$ that we studied—specifically, $\delta/t = 0.2, 0.3, 0.4, 0.5, 0.7$—we found a near saturation of $T_c(L)$ for the two largest system sizes studied, i.e., $L = 12$ and $L = 14$ for $0.4 \leqslant \delta/t \leqslant 0.8$, and $L = 10$ and $L = 12$ for $0.2 \leqslant \delta/t \leqslant 0.3$. We verified that the reason for this behavior is that the superfluid density curves for the two largest system sizes agree within statistical error bars near the BKT transition. We illustrate this behavior for the case $\delta/t = 0.4$ in Fig. 10(b). Therefore, for these band dispersions, we estimate the thermodynamic value for the transition temperature to be given by $T_c(L_{\max})$.

For the band dispersion with $\delta/t = 0.6$, even though $T_c$ nearly saturates for the two largest system sizes, the corresponding superfluid density curves are not on top of

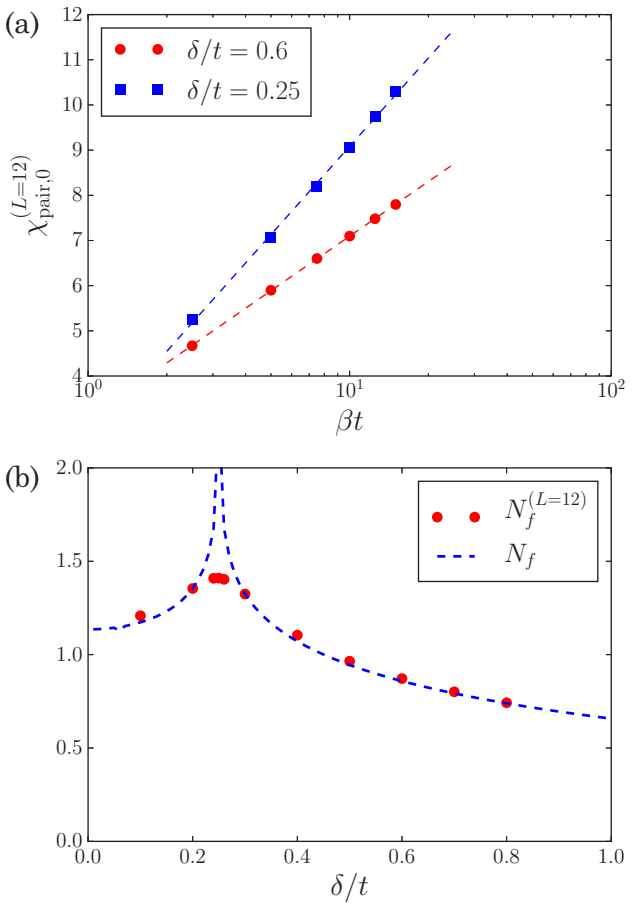


FIG. 11. (a) $\chi_{\text{pair},0}^{(L=12)}$ of the finite-size system $L = 12$ plotted as a function of the inverse temperature $\beta$ (in units of $1/t$) at the Van Hove point ($\delta/t = 0.25$) and at $\delta/t = 0.6$. (b) Comparison between the density of states of the finite-size system, $N_f^{(L=12)}$, and the density of states computed analytically, $N_f$. The results match except very close to the Van Hove singularity, where the divergence is cut off by finite-size effects.

each other within the QMC statistical error bars. This is also the case for the band dispersion with $\delta/t = 0.8$, as shown in Fig. 10(c). Moreover, for this band dispersion, $T_c$ does not really seem to saturate for the two largest system sizes, as shown in Fig. 10(a). For these two systems, $T_c(L_{\max})$ should therefore be understood as an upper bound value for the thermodynamic value of $T_c$. In these cases, we can also estimate the lower bound value by the condition that the $\rho_s(T, L_{\max})$ curve becomes larger than $\rho_s(T, L)$ for one of the smaller system sizes studied (in our case, $L = 12$). Such a criterion is based on the fact that, in the disordered phase, finite-size effects generally make $\rho_s(T, L)$ larger for smaller system sizes. The extracted lower boundary values for $T_c$ are depicted as the stars in Fig. 3 of the main text. Clearly, the only system where finite-size effects are more pronounced is the one with $\delta/t = 0.8$.

#### 4. Density of states of the finite-size system

Here we demonstrate that the bare pairing susceptibility $\chi_{\text{pair},0}$ in our simulations is sensitive to the proximity to the Van Hove singularity, despite the modest sizes of the systems. From Eq. (A27), we have

$$\chi_{\text{pair},0}(\beta) = 2N_f \ln \Lambda\beta, \tag{B9}$$

where $\Lambda$ is an upper cutoff related to the band structure. In Fig. 11(a), we show the exactly calculated pairing susceptibility for a system of size $L = 12$, $\chi_{\text{pair},0}^{(L=12)}$. We also show linear fittings to the expression above, from which we can extract the density of states of the finite-size system, $N_f^{(L=12)}$. In Fig. 11(b), we compare $N_f^{(L=12)}$ to the analytically calculated $N_f = -\frac{4}{\pi}\sum_{\mathbf{k}} \lim_{\delta\to 0_+} G(\mathbf{k}, i\delta)$ as a function of $\delta/t$. The factor of 4 arises from spin and band degeneracies. The agreement between $N_f^{(L=12)}$ and $N_f$ is evident, and the only effect of the finite size of the system is to cut off the divergence of $N_f$ at the Van Hove point.

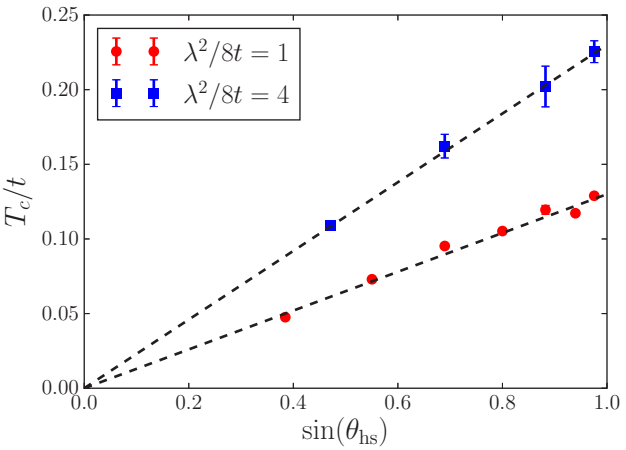


FIG. 12. $T_c$ as a function of $\sin(\theta_{\text{hs}})$ for $\lambda^2/8t = 1$, where $T_c$ scales with $\lambda^2$, and $\lambda^2/8t = 4$, where $T_c$ is in the saturation regime (see Fig. 5 of the main text). The linear dependence of $T_c$ on $\sin\theta_{\text{hs}}$ remains robust for larger values of the interaction parameter $\lambda$. The results in this figure are obtained for $L = 12$.

#### 5. Behavior of $T_c$ for larger interaction parameters

To complement the discussion in Fig. 5 of the main text, in Fig. 12 we present $T_c$ as a function of $\sin\theta_{\text{hs}}$ for both $\lambda^2/8t = 1$ and $\lambda^2/8t = 4$, which is the largest interaction parameter studied. For the latter, $T_c$ is in the saturation regime, as shown in Fig. 5 of the main text. Note, however, that $T_c$ is still linearly proportional to $\sin\theta_{\text{hs}}$, without any enhancements due to the Van Hove singularity at $\delta/t = 0.25$. Interestingly, the extension of the hot-spots Eliashberg calculation discussed in Eq. (A19) still predicts a linear dependence of $T_c$ with $\sin\theta_{\text{hs}}$ even when $T_c$ becomes independent of $\lambda$.


[1] K. Miyake, S. Schmitt-Rink, and C. M. Varma, Phys. Rev. B **34**, 6554 (1986).
[2] D. J. Scalapino, E. Loh, Jr., and J. E. Hirsch, Phys. Rev. B **34**, 8190 (1986).
[3] P. Monthoux, A. V. Balatsky, and D. Pines, Phys. Rev. Lett. **67**, 3448 (1991).
[4] P. J. Hirschfeld, M. M. Korshunov, and I. I. Mazin, Rep. Prog. Phys. **74**, 124508 (2011).
[5] Y. Dagan, M. M. Qazilbash, C. P. Hill, V. N. Kulkarni, and R. L. Greene, Phys. Rev. Lett. **92**, 167001 (2004).
[6] L. Taillefer, Annu. Rev. Condens. Matter Phys. **1**, 51 (2010).
[7] J. G. Analytis, H-H. Kuo, R. D. McDonald, M. Wartenbe, P. M. C. Rourke, N. E. Hussey, and I. R. Fisher, Nat. Phys. **10**, 194 (2014).
[8] E. M. Motoyama, G. Yu, I. M. Vishik, O. P. Vajk, P. K. Mang, and M. Greven, Nature (London) **445**, 186 (2007).
[9] T. Shibauchi, A. Carrington, and Y. Matsuda, Annu. Rev. Condens. Matter Phys. **5**, 113 (2014).
[10] A. Abanov, A. V. Chubukov, and J. Schmalian, Adv. Phys. **52**, 119 (2003).
[11] B. Kyung, J.-S. Landry, and A.-M. S. Tremblay, Phys. Rev. B **68**, 174502 (2003).
[12] M. A. Metlitski and S. Sachdev, Phys. Rev. B **82**, 075128 (2010).
[13] K. B. Efetov, H. Meier, and C. Pépin, Nat. Phys. **9**, 442 (2013).
[14] Y. Wang, A. G. Abanov, B. L. Altshuler, E. A. Yuzbashyan, and A. V. Chubukov, Phys. Rev. Lett. **117**, 157001 (2016).
[15] A. J. Millis, Phys. Rev. B **45**, 13047 (1992).
[16] H. v. Löhneysen, A. Rosch, M. Vojta, and P. Wölfle, Rev. Mod. Phys. **79**, 1015 (2007).
[17] N. Bulut, D. J. Scalapino, and S. R. White, Phys. Rev. B **47**, 2742 (1993).
[18] T. A. Maier, M. Jarrell, T. C. Schulthess, P. R. C. Kent, and J. B. White, Phys. Rev. Lett. **95**, 237001 (2005).
[19] K. Haule and G. Kotliar, Phys. Rev. B **76**, 104509 (2007).
[20] E. Gull, O. Parcollet, and A. J. Millis, Phys. Rev. Lett. **110**, 216405 (2013).
[21] S.-S. Lee, Phys. Rev. B **80**, 165102 (2009).

[22] D. F. Mross, J. McGreevy, H. Liu, and T. Senthil, Phys. Rev. B **82**, 045121 (2010).
[23] S. Raghu, G. Torroba, and H. Wang, Phys. Rev. B **92**, 205104 (2015).
[24] E. Berg, M. A. Metlitski, and S. Sachdev, Science **338**, 1606 (2012).
[25] Y. Schattner, M. H. Gerlach, S. Trebst, and E. Berg, Phys. Rev. Lett. **117**, 097002 (2016).
[26] Z.-X. Li, F. Wang, H. Yao, and D.-H. Lee, arXiv:1512.04541.
[27] Ar. Abanov, A. V. Chubukov, and M. R. Norman, Phys. Rev. B **78**, 220507 (2008).
[28] Z.-X. Li, F. Wang, H. Yao, and D.-H. Lee, Science Bulletin **61**, 925 (2016).
[29] Y. Schattner, S. Lederer, S. A. Kivelson, and E. Berg, Phys. Rev. X **6**, 031028 (2016).
[30] P. T. Dumitrescu, M. Serbyn, R. T. Scalettar, and A. Vishwanath, Phys. Rev. B **94**, 155127 (2016).
[31] J. Kang and R. M. Fernandes, Phys. Rev. B **93**, 224514 (2016).
[32] M. H. Gerlach, Y. Schattner, E. Berg, and S. Trebst, Phys. Rev. B **95**, 035124 (2017).
[33] A. V. Chubukov and J. Schmalian, Phys. Rev. B **72**, 174520 (2005).
[34] R. J. Radtke, K. Levin, H.-B. Schüttler, and M. R. Norman, Phys. Rev. B **48**, 15957 (1993).
[35] E. Fradkin, S. A. Kivelson, and J. M. Tranquada, Rev. Mod. Phys. **87**, 457 (2015).
[36] S. Badoux, W. Tabis, F. Laliberté, G. Grissonnanche, B. Vignolle, D. Vignolles, J. Béard, D. A. Bonn, W. N. Hardy, R. Liang, N. Doiron-Leyraud, L. Taillefer, and C. Proust, Nature (London) **531**, 210 (2016).